Laterally organized carbon nanotube arrays based on hot-filament chemical vapor deposition

Ki Hwan Kim, Emmanuel Lefeuvre, Marc Châtelet, Didier Pribat, Costel Sorin Cojocaru

Thin Solid Films
519 (2011) 4598–4602
DOI: http://dx.doi.org/10.1016/j.tsf.2011.01.334

Laterally organized carbon nanotube arrays based on hot-filament chemical vapor deposition

Ki-Hwan Kim [a,*], Emmanuel Lefeuvre [a], Marc Châtelet [a], Didier Pribat [a,b], Costel Sorin Cojocaru [a]

[a] Laboratoire de Physique des Interfaces des Couches Minces (LPICM), UMR 7647, Ecole polytechnique, 91128, Palaiseau CEDEX, France
[b] Departement of Energy Science, Sungkyunkwan University, Suwon, 440–746, Republic of Korea

Keywords:
Porous anodic alumina
Carbon nanotubes
Hot-filament chemical vapor deposition

ABSTRACT

Lateral porous anodic alumina (PAA) templates were used to organize carbon nanotubes (CNTs) grown by a hot-filament assisted chemical vapor deposition (HFCVD) process. For the CNT growth, we used a modified "home-made" HFCVD system with two independently powered filaments which are fitted respectively on the methane (CH_4) gas line, which serves as a carbon precursor and on the hydrogen (H_2) gas line, which acts as an etching agent for the parasitic amorphous carbon. Various activation powers of the hot filaments were used to directly or indirectly decompose the gas mixtures at relatively low substrate temperatures. A parametric study of the HFCVD process has been carried out for optimizing the confined CNTs growth inside the lateral PAA templates.

1. Introduction

Since Iijima's [1] first observation of carbon nanotubes (CNTs) in 1991, these quasi one-dimensional nanostructures have attracted much attention due to their inherent structural uniqueness, their extraordinary electronic properties and their chemical stability. CNTs have been regarded as a very promising material for next generation electronics [2] and for a proof of concept practical application, a field-effect transistor based on single-walled carbon nanotubes, was demonstrated as early as 1998 [3,4], this was followed by many studies which were motivated by the tremendous electronic characteristics [5] of such devices. Since then, CNTs have been proposed for various other electronic applications such as interconnects [6], gas sensors [7], bolometric devices [8], and photodetectors [9].

Up to now, a considerable effort has been devoted to bring such CNT-based devices to real-life application, but several hurdles still have to be overcome, which include chirality control, uniform diameter distribution, and CNT alignment. While individual CNTs exhibit excellent electronic properties, most practical applications require them to be uniformly organized (in parallel) in order to obtain high, and uniform current carrying capacity. For example, the usual current density of a conventional bulk silicon MOSFET is about 1 mA/μm [10], and one individual CNT can only carry several μA [11] despite its very high current density capacity. As a result, achieving a high and adaptable current density in CNT-based devices remains one of the most important issues for practical CNT applications. We propose to control the CNT diameter distribution and alignment, and to collectively organize them into high density regular arrays by the use of a special template, a lateral porous anodic alumina (PAA) membrane, which can be fabricated by a simple anodization process.

After its first introduction [12] in the 1950s, the properties of porous alumina templates have been the object of many studies that proved that its structure is dependent on several processing parameters factors such as the type and concentration of the electrolyte, the anodization voltage, and the process temperature and duration [13]. Among these, the anodization voltage (U) is the most dominant factor for the formation of the porous alumina structure, and determines both the pore diameter (D_p) and the interpore distance (D_{int}) (typically, $D_p = k_1 U$ and $D_{int} = k_2 U$, where $k_1 \sim 1.29$ nm/V and $k_2 \sim 2.5$ nm/V) [14]. In recent studies, we have shown that the anodic oxidation of insulator encapsulated Al thin films may allow one to fabricate a lateral type PAA structure (i.e. a porous structure developed parallel to the in-plane direction) which is more suitable for the conventional semiconductor industry [15]. In spite of such an encapsulation inducing slightly different behaviors upon anodization, we show that the same general trends and influencing parameters are to be considered for the lateral-type porous alumina anodization process as in the classical anodization process [16]. Moreover, our previous study has shown that the barrier layer at the bottom of the pores which hinders proper metal catalyst filling inside the pores through an electrodeposition process, can be thinned to a uniformly distributed thickness over the entire substrate by the use of a specifically designed exponential voltage decrease process [17]. As a next step, in this paper we report recent progress for successful carbon nanotube (CNT) growth inside of such lateral nanopore arrays.

2. Experimental

2.1. Preparation of lateral porous anodic alumina (PAA) template

The basic steps for fabricating lateral type PAA templates has been previously reported [15], and Fig. 1(a) shows a schematic image of the organized CNTs inside of a lateral PAA template. Here, we used 200 nm thick aluminum layers deposited on Si wafers with a 500 nm thick thermally grown silicon oxide layer. After patterning, the aluminum stripes were encapsulated with a 500 nm thick silicon nitride layer deposited by rf-PECVD. Prior to the anodization process, in order to achieve a flat aluminum face [15,18], we carried out a modified electropolishing process using a diluted conventional solution (1:4 volume ratio between perchloric acid and ethanol) to decrease the polishing rate. Subsequently, we carried out a classical 2-step anodization process [19] to grow an ordered nanopore array which is an important issue for further processing. The anodization process was carried out in 0.3 M oxalic acid ($H_2C_2O_4$) at 40 V, and room temperature. After the first anodization step for 1 h, we selectively etched the roughly grown PAA layer using a chromic acid contained solution (0.17 M CrO_3 + 0.6 M H_3PO_4) at 60 °C for 30 min. The second anodization step was then carried out using the same conditions as for the first step. Subsequently, a barrier layer thinning process was carried out using an exponential voltage decrease process [17] to form a uniformly distributed and sufficiently thinned barrier layer at the bottom of the pores. Following an additional pore widening process in 0.3 M phosphoric acid (H_3PO_4) at 30 °C for 25 min, the barrier oxide layer could be uniformly removed.

Prior to the CVD growth of CNTs, the nanopores were filled with Ni catalyst nanoparticles by a pulsed electrodeposition (PED) process using nickel ions contained in an electrolyte. The nickel deposition was carried out in conventional watts bath, which is a mixed solution of 330 g/L nickel sulfate hexahydrate ($NiSO_4 \cdot 6H_2O$), 45 g/L nickel chloride hexahydrate ($NiCl_2 \cdot 6H_2O$), and 38 g/L boric acid (H_3BO_3). Depending on the barrier layer thickness at the bottom of the pores, the deposition voltage had to be modified to properly fill the pores with catalyst, and the pulse shape had to be designed for improved uniformity of the catalyst filling. The number of pulse sweeps was found to influence only the final volume of the electrodeposited metal nanoparticles.

2.2. Growth process of carbon nanotubes (CNTs)

The CNT growth has been performed in a "homemade" hot-filament assisted chemical vapor deposition (HFCVD) system. The two independently powered filament's set up has been previously described, as shown in Fig. 1(b) [20]. Methane (CH_4) was used as a

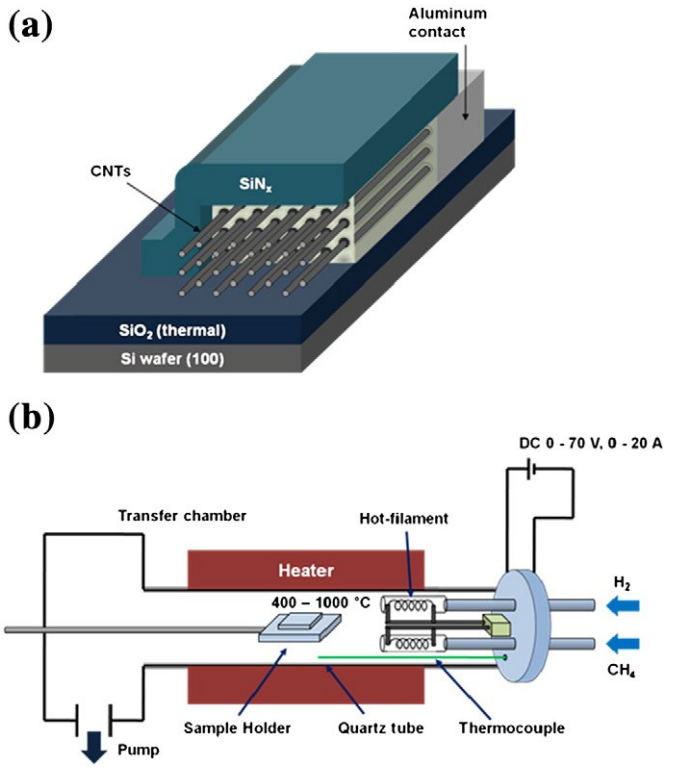

Fig. 1. Schematic diagram of (a) organized carbon nanotubes (CNTs) inside of lateral porous anodic alumina (PAA) template after CNT growth process, and (b) the hot-filament chemical vapor deposition (HFCVD) set-up. Ideally grown CNTs have very straight and defectless quasi-1D nanostructure, but organized CNTs outside of template show slightly entangled and branched structure in this case.

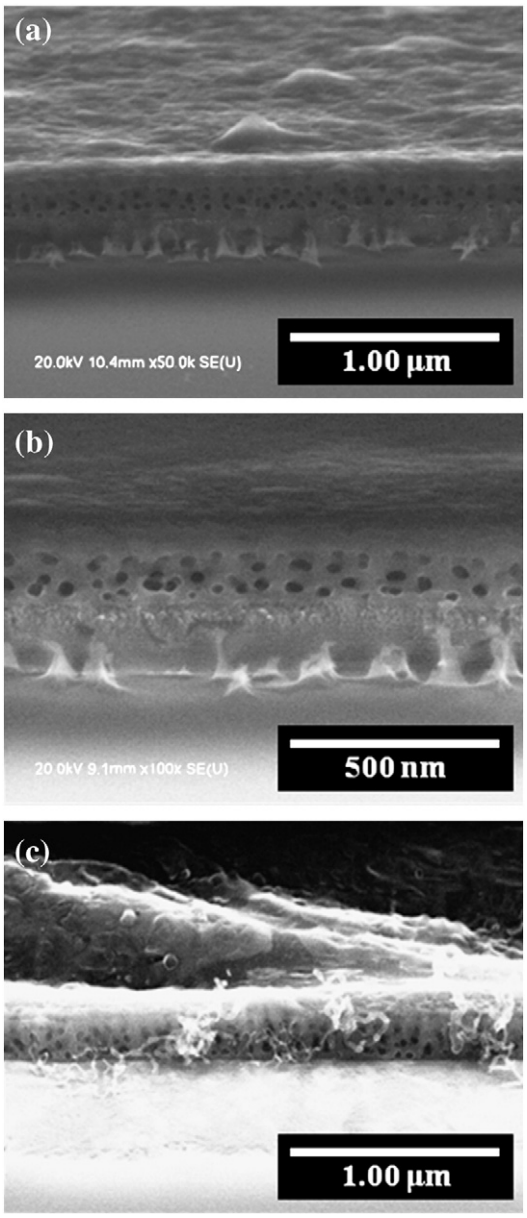

Fig. 2. Scanning electron microscope (SEM) images of grown CNTs at 600 °C using (a) 10 sccm CH_4:90 sccm H_2, 95 mbar with 125 W filament power, (b) 20 sccm CH_4:80 sccm H_2, 95 mbar with 125 W filament power, (c) 50 sccm CH_4:50 sccm H_2, 95 mbar with 125 W filament power.

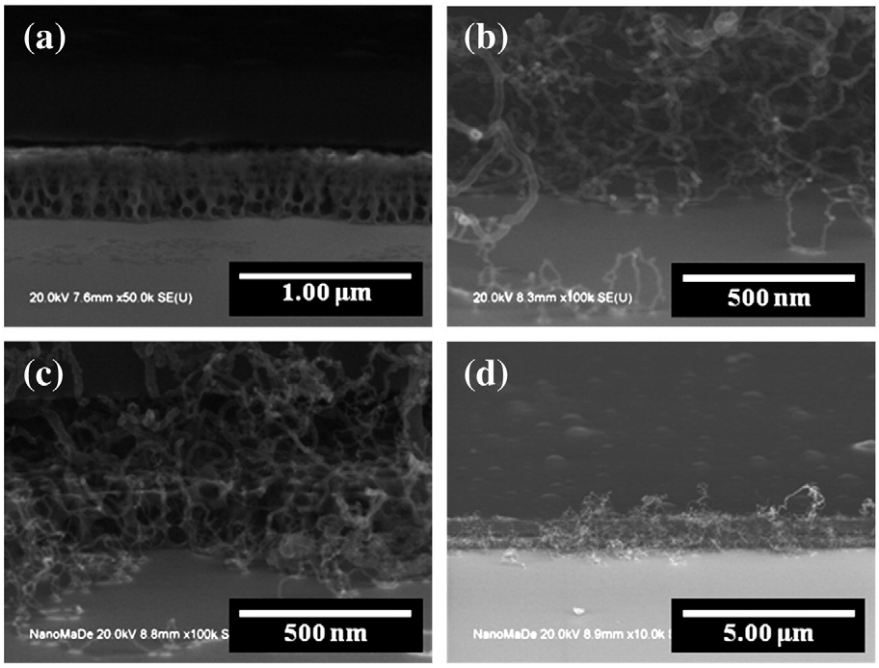

Fig. 3. SEM images of grown CNTs with 50 sccm CH_4:50 sccm H_2 at 600 °C, (a) 50 mbar with 125 W filament power, (b) 50 mbar with 205 W filament power, (c) 25 mbar with 205 W filament power, and (d) 10 sccm CH_4:90 sccm H_2, 95 mbar with 205 W filament power for 30 min after H_2 reduction process.

carbon precursor feedstock, with H_2 acting as an etching agent for scavenging the parasitic amorphous carbon (a-C) deposition during CNT growth.

The CNT growth was divided in two steps. For the first step, after increasing the furnace temperature to the target temperature, H_2 is introduced into the deposition chamber in order to perform catalyst reduction under an activated atomic hydrogen flow generated by the hot filament. In the second step, the effective CNT growth starts after introducing CH_4. Various CH_4/H_2 gas compositions have been explored, and we optimized some other parameters such as the process pressure, and the filament activation power for the gas precursor decomposition. We also examined the effect of the H_2 treatment effect before initiating CNT growth, and the effect of the temperature on CNT growth.

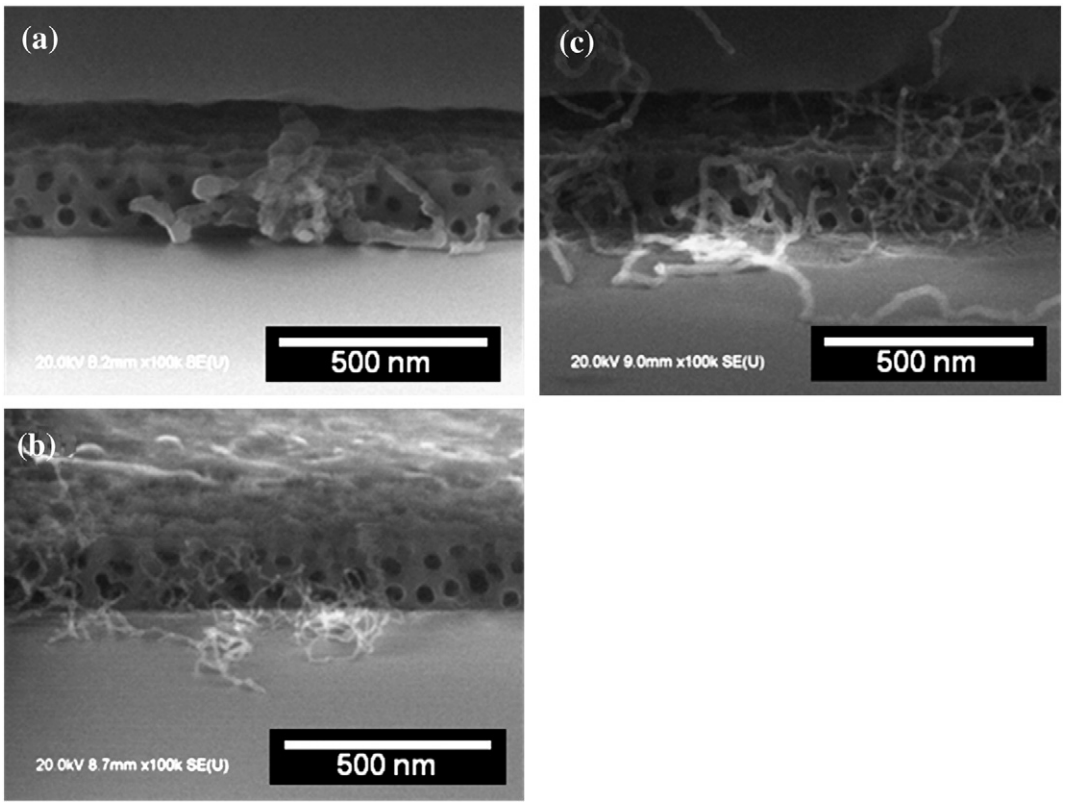

Fig. 4. SEM images of grown CNTs with treated various hydrogen reduction time before CNT growth process. (a) 2 min, (b) 15 min, (c) 30 min.

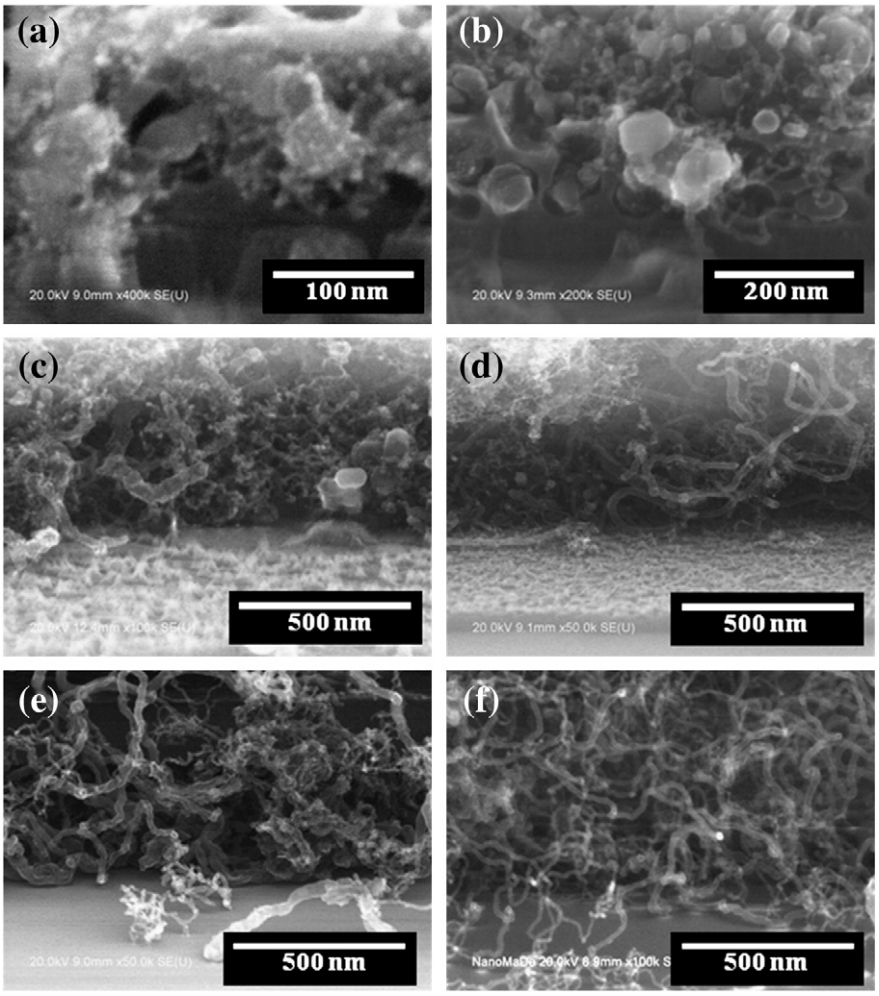

Fig. 5. SEM images of grown CNTs at various growth temperature. (a) 350 °C, (b) 400 °C, (c) 450 °C, (d) 500 °C, (e) 550 °C, and (f) 600 °C. Every CNT growth was carried out at 50 mbar, with 180 W for 30 min. Gas composition ratio was 50:50 (sccm) between CH_4 and H_2.

The as grown CNTs could be observed by field emission scanning electron microscopy (FESEM, HITACHI S4800) and their quality characterized using Raman spectroscopy.

3. Results and discussion

Due to the particular morphology of the lateral PAA templates, and resulting in catalyst confinement inside the nanopores with a high aspect ratio, the parameters for CNT growth are strongly modified with respect to the CVD growth conditions on conventional plane substrates.

We started the CNT growth optimization at 600 °C, 95 mbar total pressure, and 125 W activation power for the H_2 filament, while varying the gas mixture composition ratio from 10% to 50% CH_4 for a fixed total gas flow of 100 sccm. The relatively low CH_4/H_2 ratio was required to prevent parasitic amorphous carbon (a-C) deposition on the lateral PAA template surface. The results are summarized in Fig. 2 and one can notice that little or no CNT deposition occurred when using low CH_4/H_2 ratios (Fig. 2(a), (b)). We attribute this behavior to the insufficient activation of the carbon precursor (low growth temperature and low hot filament power activation). Only at relatively high CH_4/H_2 ratio (50%) were the radicals/molecules sufficiently activated to reach the Ni catalyst nanoparticles at the bottom of the nanopores, resulting in grown CNT growth from inside of the nanopores as this is seen in Fig. 2(c). This behavior was further confirmed by lowering the total pressure during deposition (while keeping the 50% CH_4 ratio). As can be seen in Fig. 3(a), no CNT growth could be observed.

Fig. 3 summarizes the results for CNT growth at various process pressures, and various gas composition ratios with high filament power. Similar to the results for the gas composition ratio, if the process pressure is low, the precursor molecule activation/dissociation rates through the hot filament are substantially reduced, thus strongly impacting the CNT growth. However, when the filament activation power is increased sufficiently (up to 205 W − 1900 °C), we could observe CNTs growing from inside of the pores, as shown in Fig. 3(b). Once methane molecules are sufficiently decomposed, CNTs could be easily grown even at lower methane partial pressures (lower process pressures, and lower CH_4/H_2 ratio), as shown in Fig. 3(c), and (d). These experimental results point out the important role of the hot filament activation, and following these trends, we could extend these results to more harsh growth conditions such as extremely low process temperatures, process pressures, and gas composition ratios.

Successful CNT growth inside lateral PAA templates is conditioned not only by the HFCVD growth conditions which represent the second step of our growth process, but also by the catalyst reduction process under hot-filament activated hydrogen. After catalyst filling inside of the lateral PAA, the catalytic metal nanoparticles can normally be easily oxidized and thus cannot be readily activated for subsequent CNT growth. In order to enhance the catalytic activity of the filled metals, we carried out a distinct reduction process through prolonged exposure to a hot filament activated hydrogen flow. As the duration of

this reduction step was increased, we could observe a clear improvement of CNT growth density inside the lateral PAA pores, as summarized in Fig. 4. We suggest that the prolonged duration of the reduction step helps activate an extended number of oxidized catalyst nanoparticles. As a result, suitably activated catalytic nanoparticles lead to more efficient dissociation of the carbon precursor, and increase the yield of CNT growth.

The CNT growth temperature is another important parameter. Even though the decomposition of gas molecules takes place mainly at the thermally activated filament level, the substrate temperature is important because it influences the dissociative adsorption of the molecules at the catalyst level as well as the diffusion of carbon atoms into the metal. Since we use porous alumina templates obtained by partial anodic oxidation of encapsulated aluminum stripes, the CNT growth process is limited to a relatively low temperature (b 650 °C), not only to prevent the remaining aluminum layers from melting but also to minimize the thermal expansion difference which induces cracks on the capping layer. Fortunately, as mentioned above, for the HFCVD process, the carbon feedstock can be pre-decomposed through activated hot filaments, so the substrate temperature could be lowered compared to the "classical" thermal CVD process. The results we obtained at various growth temperatures are summarized in Fig. 5.

One can notice (Fig. 5(a)) that our process allows for some CNT-like structures to grow even at substrate temperatures as low as 350 °C. However, for temperatures below 400 °C (Fig. 5(b)), the hot filament activation is no longer sufficient and the growth rate gets too low to yield good quality CNTs. In both cases (Fig. 5(a), and (b)), we just observe CNTs which are in their initial growth stage. We note in these images that in some parts of the lateral PAA, nickel catalyst over-deposition took place due to increased number of pulse sweeps during the electrodeposition process. Fortunately, on such over-deposited nickel particles, we observe some CNTs that appear in an incipient growth stage. On the other hand, starting from 500 °C (Fig. 5(e)), we could notice relatively straight and long CNTs growing from the lateral PAA template. As CNTs are envisioned as a channel between two electrodes for devices such as interconnects, field-effect transistors, sensors and so on, we point out that such lateral PAA grown CNTs at 500 °C can be utilized as a channel for further integration into electronic devices.

4. Conclusion

We have successfully developed a hot-filament chemical vapor deposition (HFCVD) process to grow carbon nanotubes (CNTs) inside lateral-type porous anodic alumina templates at growth temperatures ranging from 600 °C to as low as 350 °C. Such CNT arrays can be used as a channel for further development of electronic applications such as interconnects, field-effect transistors, sensors, photonic devices and so on. The parametric study of the growth process pointed out that the gas composition ratios and the hot filament activation power strongly impact the CNT growth. Moreover, a specific catalyst reduction/activation step has been successfully implemented for improving the CNT growth yield.

References

[1] S. Iijima, Nature 354 (1991) 56.
[2] R. Saito, G. Dresselhaus, M.S. Dresselhaus, Physical Properties of Carbon Nanotubes, Imperial College Press, London, 1998.
[3] S.J. Tans, A.R.M. Verschueren, C. Dekker, Nature 393 (1998) 49.
[4] R. Martel, T. Schmidt, H.R. Shea, T. Hertel, Ph. Avouris, Appl. Phys. Lett. 73 (17) (1998) 2447.
[5] A. Javey, J. Guo, Q. Wang, M. Lundstrom, H.J. Dai, Nature 424 (2003) 654.
[6] J. Li, Q. Ye, A. Cassell, H.T. Ng, R. Stevens, J. Han, M. Meyyappan, Appl. Phys. Lett. 82 (2003) 2491.
[7] A. Modi, N. Koratkar, E. Lass, B. Wei, P.M. Ajayan, Nature 424 (2003) 171.
[8] M.E. Itkis, F. Borondics, A. Yu, R.C. Haddon, Science 312 (5772) (2006) 413.
[9] M. Freitag, Y. Martin, J.A. Misewich, R. Martel, P.H. Avouris, Photoconductivity of Single Carbon Nanotubes, vol. 3, No. 8, 2003, p. 1067.
[10] At the 2008 IEDM conference (15–17 December), Intel announced 1.55 mA/μm for NMOS and 1.21 mA/μm for PMOS transistors, using their 32 nm platform.
[11] A. Javey, H. Kim, M. Brink, Q. Wang, A. Ural, J. Guo, P. McIntyne, P. McEuen, M. Lundstrom, H.J. Dai, Nat. Mater. 1 (2002) 241.
[12] F. Keller, M.S. Hunter, D.L. Robinson, J. Electrochem. Soc. 100 (1953) 411.
[13] J.P. O'Sullivan, G.C. Wood, The morphology and mechanism of formation of porous anodic films on aluminium, 317, 1970, pp. 511–543.
[14] K. Nielsch, J.S. Choi, K. Schiwirn, R.B. Wehrspon, U. Gösele, Nano Lett. 2 (7) (2002) 677.
[15] C.-S. Cojocaru, J.M. Padovani, T. Wade, C. Mandoli, G. Jaskierowicz, J.E. Wegrowe, A.F. Morral, D. Pribat, Nano Lett. 5 (4) (2005) 675.
[16] M. Gowtham, L. Eude, C.-S. Cojocaru, B. Marquardt, H.J. Jeong, P. Legagneux, K.K. Song, D. Pribat, Nanotechnology 19 (2008) 035303.
[17] B. Marquardt, L. Eude, M. Gowtham, G.S. Cho, H.J. Jeong, M. Chatelet, C.-S. Cojocaru, B.S. Kim, D. Pribat, Nanotechnology 19 (2008) 405607.
[18] R.E. Ricker, A.E. Miller, D.-F. Yue, G. Banerjee, S. Bandyopadhyay, J. Electron. Mater. 25 (10) (1996) 1585.
[19] H. Masuda, K. Fukuda, Science 268 (1995) 1466.
[20] H.J. Jeong, L. Eude, M. Gowtham, B. Marquardt, S.H. Lim, S. Enouz, C.-S. Cojocaru, Y.H. Lee, D. Pribat, Nano 3 (2008) 145.